Pergamon

Int. J. Solids Structures Vol. 33, No. 16, pp. 2309–2329, 1996

0020–7683/96 $15.00 + .00

0020–7683(95)00155–7

A HYBRID MICRO-MACRO BEM WITH MICRO-SCALE INCLUSION-CRACK INTERACTIONS

Z. Q. JIANG, A. CHANDRA and Y. HUANG
Department of Mechanical Engineering and Engineering Mechanics,
Michigan Technological University, Houghton, MI 49931-1295, U.S.A.

(*Received* 2 *October* 1994; *in revised form* 12 *September* 1995)

Abstract—Local analysis schemes capable of detailed representations of micro-features of a problem are integrated with a macro-scale BEM technique capable of handling finite geometries and realistic boundary conditions. This paper focuses on micro-scale interactions among cracks and inclusions as well as their ramifications on macro-scale damage evaluations. The micro-scale effects are introduced into the macro-scale BEM computations through an augmented fundamental solution obtained from an integral equation representation of the micro-scale features. The proposed hybrid micro-macro BEM formulation allows complete decomposition of the real problem into two sub-problems, one residing entirely at the micro-level while the other resides at the macro-level. This allows for investigations of the micro-structural attributes while retaining the macro-scale geometric features and actual boundary conditions for the structural component under consideration. As a first attempt, dilute inclusion densities with strong inclusion-crack and crack-crack interactions are considered. The numerical results obtained from the hybrid BEM analysis establish the accuracy and effectiveness of the proposed micro-macro computational scheme for this class of problems. The proposed micro-macro BEM formulation can be easily extended to investigate the effects of other micro-features (e.g., interfaces, short or continuous fibers, in the context of linear elasticity) on macro-scale failure modes observed in structural components. Copyright © 1996 Elsevier Science Ltd.

1. INTRODUCTION

Many engineering materials contain defects in the form of cracks, voids and inclusions that can significantly affect their load carrying capabilities. Damage is easily initiated as micro-cracks around an inclusion due to the residual stresses and thermal mismatch between inclusion and matrix properties. Accordingly, interactions among these micro-scale defects play crucial roles in determining the strength and life of components under service conditions. This is particularly true for relatively brittle materials such as ceramics, intermetallics or ceramic matrix composites.

In recent years, performance and weight goals for the next generation of high-temperature applications have spurred the development of improved intermetallics and ceramic matrix composites capable of sustained operations in the 1000–1500°C range. These materials contain multiple phases and secondary phase particles. To model real-life applications of these high-temperature components, one must incorporate general loading situations, finite and often complex geometries of particular components, and detailed representations of interacting inhomogeneities, along with their associated damage evolutions. And therein lies the fundamental difficulty in the analysis of these problems. Typically, the micro-defects and their spacings are of the order of a few micrometers while the overall dimensions of a component may range from a few centimeters to even a meter. Thus, the computational scheme is required, simultaneously, to provide a detailed representation of the underlying mechanics at two widely different scales: a local micro-scale ranging from 10 to 100 μm and a global macro-scale that may range from 10 to 1000 mm.

The computational techniques in existence today, such as the finite element method (e.g., Oden (1972), Gallagher (1975), Bathe (1982), and Zienkiewicz and Taylor (1991)) and the boundary element method (e.g., Banerjee and Butterfield (1981), Mukherjee (1982), Cruse (1988), Lutz *et al.* (1992), and Huang and Cruse (1994)), are ideally suited for macro-scale analysis and can easily handle complex geometries along with general loading conditions. Thus, the defects are normally introduced as geometric entities in such macro-scale computational schemes. The resulting mixed boundary value problems essentially

assume that the defect sizes are of the same order as the geometric dimensions of the body (e.g., Cruse and Polch (1986)). In many cases, special quarter-point finite elements (e.g., Barsoum (1976), Yahia and Shephard (1985)) or boundary elements (e.g., Crouch (1976), Kamel and Liaw (1991a,b), and Raveendra and Banerjee (1992)) are introduced to capture the $\sqrt{r}$ singularity at the tip of an elastic crack. Snyder and Cruse (1975) have developed numerical fundamental solutions for fracture problems. Cruse and Novati (1992) have also utilized a displacement discontinuity approach to formulate a traction BIE formulation for nonplanar and multiple crack problems. In such cases, the details of micro-scale features are limited by the level of discretization, and the technique becomes prohibitively expensive if a large number of micro-features need to be represented. Moreover, such a technique is applicable only to isolated elastic cracks. These special elements cannot represent any effects due to crack interactions, and one must rely on numerical discretization to capture such effects. This poses significant difficulties whenever the cracks are closely packed. Besides, these special elements cannot be directly extended to model other types of defects, such as voids or inclusions (e.g., secondary phases and short or continuous fibers) that are commonly present in many real materials. And, an understanding of the evolution of such defects in a damage cluster is critically important for estimating the characteristics (e.g., strength and fracture toughness) of modern intermetallics and ceramic materials.

Over the last decade or so, several researchers (e.g., Tvergaard (1982, 1989a,b, 1990); Needleman (1987), Fleck *et al.* (1989); and Needleman and Tvergaard (1991)) developed a unit cell approach (under assumptions of doubly periodic defect distributions) to investigate micro-scale issues such as void growth resulting in plastic instabilities, decohesion of hard particles from the matrix material, etc., in the context of computational mechanics. Chandra and Tvergaard (1993) also utilized such a unit cell approach to investigate void nucleation and growth in plane strain extrusion processes. Feng *et al.* (1994) have also utilized unit cell representations to investigate micro-scale effects in sinter-forming processes. The unit cells, however, are by definition much smaller than the macroscopic dimensions of the body and exist essentially at a micro-scale of the same order as the defect sizes. Thus, the computations are carried out entirely at a micro-scale. Becker (1992) also carried out finite element analyses, entirely at a micro-scale, to investigate the effects of different crystallographic orientations in a polycrystalline material.

Thus, the computational techniques available today are capable of analyzing a problem at a macro-scale or at a micro-scale. They, however, cannot bridge these two widely different scales in a single analysis. Recently, Banerjee and Henry (1992) introduced special boundary elements and Nakamura and Suresh (1993) extended the unit cell analysis using FEM for modeling the effects of fiber packing in composite materials. However, much work is needed before one can directly investigate the effects of macro-scale design (geometric, loading, and boundary condition) considerations upon the evolutions of micro-scale defects, which essentially govern the strength and life of individual component in service.

Over the past few decades, analytical techniques have been used extensively to investigate various micro-mechanical phenomena. Several micro-mechanical models have been developed to study the behavior of materials containing various distributions of inhomogeneities, which may be reinforcements or defects. These approaches include self-consistent (Budiansky (1965)), differential (Roscoe (1952), Norris (1985)), Mori-Tanaka (Taya and Chou (1981), Weng (1984)), and generalized self-consistent (Christensen and Lo (1979), Huang *et al.* (1994)) methods. Micro-mechanical models are particularly suited for the prediction of overall properties of composites, but they cannot accurately represent the local stress and deformation fields around each inhomogeneity. These local fields, however, have been demonstrated to be of extreme importance for defect initiation, growth, and coalescence (Becker *et al.* (1988)).

Various researchers have attempted to investigate the interactions among micro-defects in a damage cluster. Horii and Nemat-Nasser (1986) used a pseudo-traction approach for problems involving crack interactions. Hu and Chandra (1993a,b,c) modeled the micro-crack as distributions of dislocations and the rigid lines as distributions of tractions in order to develop an integral equation approach for investigating interactions among cracks and rigid lines in a defect cluster. The approach of Hu and Chandra has also been extended to

interactions of voids, cracks, and rigid lines (Hu *et al.* (1993a)). The Gauss-Chebychev quadrature scheme (Erdogan *et al.* (1973)) utilized by Hu and Chandra (1993a,b,c) requires only n quadrature points for accurate representations of polynomial functions of order $2n$. Using such a scheme, they were able to investigate defect interactions at very close spacings. For a problem involving equal-length collinear cracks with a small tip separation of only 1% of the half-length of the crack, the scheme of Hu and Chandra (1993b) with 30 quadrature points on a crack yield SIF values within 0.1% of the analytical results of Erdogan (1962). Hu *et al.* (1993a,b, 1994) also pursued a traction approach to investigate the interactions among bridged cracks and their implications on defect coalescence in various multi-phase ceramic materials.

The analytical and semi-analytical investigations cited above can provide crucial insights into the behaviors of interacting micro-defects in a damage cluster. However, these analyses are mostly carried out under assumptions of infinite bodies or extremely simplified geometry and loading conditions, which severely restricts their applicability to real-life situations involving complex finite geometries and general loading conditions. Thus, on one hand, there are analytical models capable of yielding very accurate results for various micro-scale phenomena involving evolutions of micro-defects in a damage cluster, but for very simple geometries and loading situations. On the other hand, very powerful computational techniques have been developed to handle real-life-macro-scale problems involving complex finite geometries and general loading conditions, yet it is very difficult to relate the effects of macro-scale parameters on the interactions and evaluations of micro-features present in a real material.

To address this issue, Chandra *et al.* (1995) have recently developed a hybrid micro-macro BEM formulation capable of representing interaction effects in micro-crack clusters. The present paper extends the hybrid micro-macro BEM technique to inclusion-crack interactions. The proposed BEM formulation can handle a wide variety of harder (than matrix) or softer inclusions. Thus, a void may also be modelled as a very soft inclusion. Over the years, the necessity of a fundamental solution in a BEM analysis have traditionally been viewed as one of its weaknesses. In the present work, however, this particular feature of BEM provides an avenue for incorporating insights gained from micro-scale analytical investigations into a macro-scale computational technique. This allows us, in a single analysis, to investigate the effects of macro-scale variations in geometrical features and boundary conditions on the micro-scale evolutions of defects in damage clusters. The micro-phenomena are captured in the fundamental solution, and the conventional BEM technique is used to relate them to the macro-scale problem. Such an approach also facilitates sequential modeling of the micro-features and the macro-scale problem. Thus, it obviates the problem of proliferation of degrees of freedom that is commonly observed in computational efforts attempting to capture both micro- and macro-features of a problem.

The present paper starts with a brief exposition of some relevant analytical results. The micro-scale features of the problem are addressed next, and an integral equation technique is used to numerically construct the appropriate fundamental solution. As a first attempt, circular inclusions with dilute densities are assumed and particular attention is paid to crack-crack as well as crack-inclusion interactions. However, it should be emphasized that, following the work of Hu and Chandra (1993a,b,c) Hu *et al.* (1993a,b, 1994) and Huang (1993), fundamental solutions can also be obtained for problems involving other micro-features, e.g., fibers and interfaces and elliptic inclusions. The augmented fundamental solution is then incorporated in a direct BEM approach to solve the macro-scale elasticity problems. The numerical results obtained from the proposed hybrid micro-macro BEM formulation are first verified against available results in the literature. The capabilities of the proposed scheme are investigated, and various salient features are discussed.

2. MICRO-SCALE FUNDAMENTAL SOLUTIONS

The fundamental solutions representing the micro-features involving interacting cracks and circular inclusions are developed in this section. The macroscopic body as well as the inclusion are assumed to be elastic. In order to evaluate the augmented fundamental

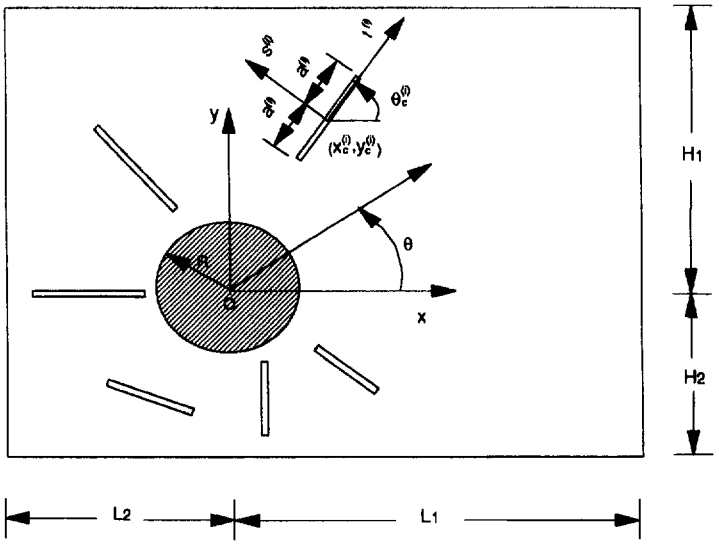

Fig. 1. A general system containing an inclusion and multiple micro-cracks.

solution for later incorporation into the macro-scale problem, the finite body with the inclusion and micro-cracks is first embedded in an infinite domain and is subjected to a point load at any desired location inside or on the boundary of the embedded finite body.

A system containing a representative micro-structure with multiple micro-cracks in the vicinity of a circular inclusion is shown in Fig. 1. A global Cartesian coordinate system is chosen such that its origin is located at the center of the inclusion. The inclusion, of radius R, shear modulus G_2 and Poisson's ratio v_2, is assumed to be perfectly bonded to a matrix material with shear modulus G_1 and Poisson's ratio v_1. Around the inclusion there are M cracks in the matrix. The associated polar coordinate system is denoted by r and θ, and a local normal-tangential coordinate system corresponding to the ith crack is represented by $s^{(i)}$ and $t^{(i)}$, in which the occupancy of the ith crack is taken as $-a^{(i)} < t^{(i)} < a^{(i)}$. The geometry of the ith crack is specified by the center coordinates $(x_c^{(i)}, y_c^{(i)})$, orientation angle $\theta_c^{(i)}$, and the half length of the crack $a^{(i)}$.

In addition to satisfying the linear and angular momentum equilibrium equations, the system must also meet the continuity conditions of displacements and tractions across the inclusion-matrix interface. Moreover, the crack interface must be traction free (omitting any effects of crack closure).

Following the superposition technique utilized by Hu and Chandra (1993a,b,c), the above problem can be decomposed into two sub-problems. As shown in Fig. 2, the first sub-problem deals with the matrix embedded with the inclusion, subject to the same external loading (point load) as the original problem, but in the absence of any cracks. The second sub-problem is concerned with cracks along with the balancing tractions needed to maintain traction-free conditions along the crack surfaces for the overall problem, but subject to no external loading.

Considering the first sub-problem, the traditional technique (Banerjee and Butterfield (1981), Brebbia and Dominguez (1992)) has been to consider the inclusion as a zoned medium within matrix, discretizing the boundaries of the body, including the inclusion-matrix interface and forcing continuity of displacements and tractions along the interface. The equations formulated for both inclusion and matrix may then be solved simultaneously, once the external boundary conditions are taken into account (e.g., Banerjee and Butterfield (1981), Brebbia and Dominguez (1992)). Such an approach requires simultaneous discretizations of macro-scale external boundary as well as micro-scale inclusion and cracks interface boundaries. Typically, overall dimensions of components are 3–6 orders of magnitudes bigger than the dimensions of the micro-features, and the computational technique becomes prohibitively cumbersome if these widely different scales are included in a single analysis.

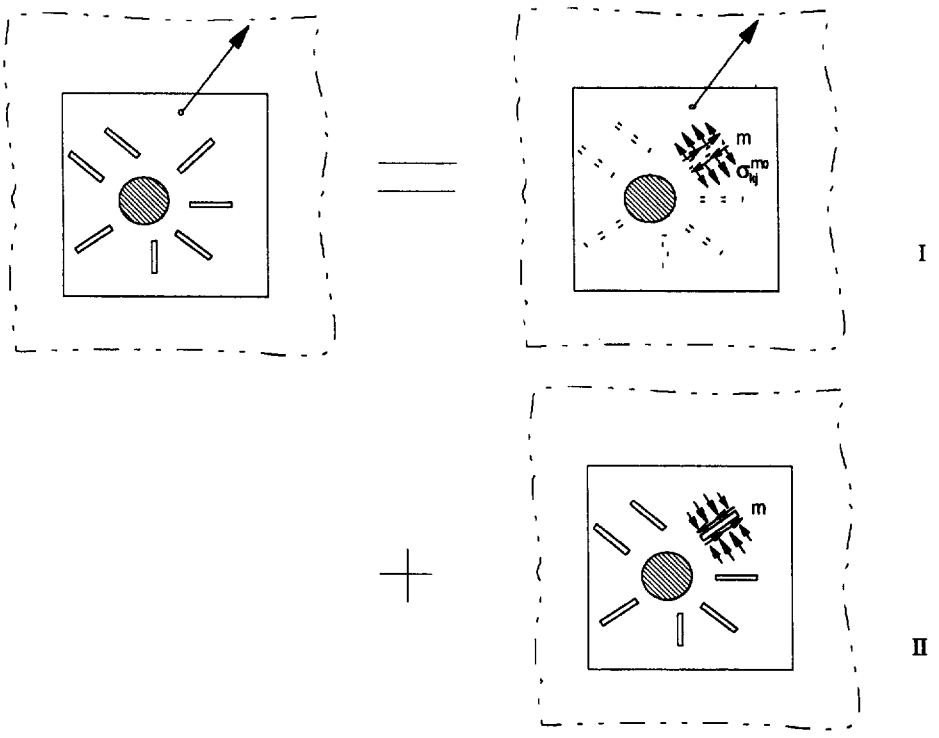

Fig. 2. Decomposition of the original problem.

A two step approach, where the first step deals with the micro-features and the second step incorporates the results from the micro-scale investigations into a macro-scale analysis is pursued in the present work. The fundamental solution provides a bridge for transition from the micro- to the macro-scale.

In the present analysis, the solution to the first sub-problem, that of a point load in an infinitely extended matrix embedded with an inclusion, is derived using the Airy stress functions (Dundurs and Hetenyi (1961), Hetenyi and Dundurs (1962)). The displacement field at a source point p may be written as

$$u_i^{(R1)}(p) = \{U_{ij}(p,q) + \bar{U}_{ij}(p,q)\}\mathbf{e}_j(q) \tag{1a}$$

and

$$\tau_i^{(R1)}(p) = \{T_{ij}(p,q) + \bar{T}_{ij}(p,q)\}\mathbf{e}_j(q) \tag{1b}$$

in which the equilibrium equations of the stress state at any point within the matrix or the inclusion as well as the interface continuity conditions are exactly satisfied. U_{ij} and T_{ij} are well known two-dimensional Kelvin solutions in the absence of any body forces and may be expressed as

$$U_{ij}(p,q) = \frac{-1}{8\pi(1-\nu)}[(3-4\nu)\ln r\delta_{ij} - r_{,i}r_{,j}] \tag{2a}$$

and

$$T_{ij}(p,q) = \frac{-1}{4\pi(1-\nu)r}\left[\{(1-2\nu)\delta_{ij} + 2r_{,i}r_{,j}\}\frac{\partial r}{\partial n} - (1-2\nu)(r_{,i}n_j - r_{,j}n_i)\right] \tag{2b}$$

$\bar{U}_{ij}$ and $\bar{T}_{ij}$ are additional parts (Hu *et al.*, 1994a) due to variation of material parameters between the matrix and the inclusion. The expressions for $\bar{U}_{ij}$ are shown in the Appendix. With the same scheme, $\bar{T}_{ij}$ can be easily derived.

In eqns (1) and (2), p and q, respectively, denote a source and a field point at an internal point while P and Q express a source and a field point on the boundary. The distance between the source and the field points is denoted by r, and $\mathbf{e}_j$ represents a unit vector. Equation (1) is written for plane strain. For plane stress, v should be substituted by $\bar{v} = v/(1+v)$. It should also be noted that U_{ij} contains a singularity of the order $\ln(r)$ and T_{ij} contains a singularity of the order $(1/r)$ as r approaches zero, and $\bar{U}_{ij}$ as well as $\bar{T}_{ij}$ are regular anywhere within the matrix. Thus, the first sub-problem may be investigated by implicitly accounting for the inclusion and without any discretization of the inclusion-matrix interface.

For the second sub-problem, following Bilby and Eshelby (1968), Atkinson (1972), Erdogan *et al.* (1974) as well as Hu and Chandra (1993a,b,c), a crack can be modeled as a continuous distribution of dislocations. We consider an infinitely extended matrix containing M interacting micro-cracks around an inclusion. The components $b_t^{(i)}$ and $b_s^{(i)}$ of the dislocation density vector along the ith crack may be expressed as,

$$b_t^{(i)}(t^{(i)}) = \frac{\partial}{\partial t^{(i)}}[u_t^{(i)}(t^{(i)}, 0^-) - u_t^{(i)}(t^{(i)}, 0^+)] = \frac{\partial \Delta_t^{(i)}(t^{(i)})}{\partial t^{(i)}} \tag{3a}$$

$$b_s^{(i)}(t^{(i)}) = \frac{\partial}{\partial t^{(i)}}[u_s^{(i)}(t^{(i)}, 0^+) - u_s^{(i)}(t^{(i)}, 0^-)] = \frac{\partial \Delta_s^{(i)}(t^{(i)})}{\partial t^{(i)}} \tag{3b}$$

where $\Delta_t^{(i)}$ and $\Delta_s^{(i)}$ represent the glide and climb movements, respectively, in the local tangential-normal $(t^{(i)}, s^{(i)})$ coordinate system for the ith micro-crack whose orientation is shown in Fig. 1.

Dundurs and Mura (1964) have investigated the problem of a two-dimensional infinite body embedded with an inclusion subjected to an edge dislocation with Burgers' vector components b_x and b_y acting at a point $(\xi, 0)$. Based on their results, a fundamental solution at (x, y) due to an edge dislocation at $(\xi, 0)$ may be obtained as (Hu *et al.* (1994a)):

$$u_i = \frac{1}{2\pi(1-\nu_1)} H_{ij}(x, y; \xi) b_j \tag{4a}$$

$$\sigma_{ij} = \frac{G_1}{\pi(1+\kappa_1)} J_{ijk}(x, y; \xi) b_k \tag{4b}$$

where G_1 is the shear modulus of matrix. The constant $\kappa_1 = (3-4\nu_1)$ for plane strain and $\kappa_1 = (3-\nu_1)/(1+\nu_1)$ for plane stress. The detail of the kernels H_{ij} are presented in the Appendix, and J_{ijk} may be found in Hu *et al.* (1994a). It is important to note here that the stress fields in eqn (4) contain a singularity of the order of r as the distance r between a field point (x, y) and a source point $(\xi, 0)$ approaches zero.

Using the same approach of Hu and Chandra (1993a,b,c) and neglecting any crack closure during the application of the external load, the governing equations for the mth crack in a system of arbitrarily oriented M interacting cracks around an inclusion may be expressed as

$$\sum_{i=1}^{M} \int_{-a^{(i)}}^{a^{(i)}} [K_{jkl}(t^{(m)}, t^{(i)}) b_l^{(i)}(t^{(i)})] \, \mathrm{d}t^{(i)} + \sigma_{jk}^{(m_0)}(t^{(m)}) = 0 \tag{5}$$

in the local tangential-normal coordinate system for the mth crack. The index j is identified as the normal direction for the mth crack. The index k refers to the local coordinates of the mth crack while the index l refers to those of the ith crack ($k, l = 1, 2$). Here, $b_l^{(i)}$ represents the unknown dislocations on the ith crack, and $\sigma_{jk}^{(m0)}$ denotes stress components at the presumed location of the mth crack due to external loading shown in the first sub-problem in Fig. 2, but in the absence of any crack. The governing eqn (5) represent the traction-free conditions at crack surfaces. The equilibrium for the resulting stress fields and continuity

conditions across the interface of inclusion and matrix are satisfied by virtue of K_{jkl}. Any tractions applied directly on the crack surfaces can also be handled by suitably modifying $\sigma_{jk}^{(m0)}$. Here, the kernels K_{jkl} in eqn (5) may be obtained by transforming the kernels J_{jkl} to an appropriate local coordinate system for the mth crack and may be expressed as,

$$K_{j11}(t^{(m)}, t^{(i)}) = \frac{G_1}{p(1+k_1)}\{[(J_{221}\cos y - J_{222}\sin y) - (J_{111}\cos y - J_{112}\sin y)]\sin f\cos f + (J_{121}\cos y - J_{122}\sin y)(\cos^2 f - \sin^2 f)\} \quad (6a)$$

$$K_{j12}(t^{(m)}, t^{(i)}) = \frac{G_1}{p(1+k_1)}\{[(J_{221}\sin y + J_{222}\cos y) - (J_{111}\sin y + J_{112}\cos y)]\sin f\cos f + (J_{121}\sin y + J_{122}\cos y)(\sin^2 f - \cos^2 f)\} \quad (6b)$$

$$K_{j21}(t^{(m)}, t^{(i)}) = \frac{G_1}{p(1+k_1)}\{(J_{111}\cos y - J_{112}\sin y)\sin^2 f + (J_{221}\cos y - J_{222}\sin y)\cos^2 f - 2(J_{121}\cos y - J_{122}\sin y)\} \quad (6c)$$

$$K_{j22}(t^{(m)}, t^{(i)}) = \frac{G_1}{p(1+k_1)}\{(J_{111}\sin y + J_{112}\cos y)\sin^2 f + (J_{221}\sin y + J_{222}\cos y)\cos^2 f - 2(J_{121}\sin y + J_{122}\cos y)\sin f\cos f\} \quad (6d)$$

where angles ψ and ϕ depend on the geometries of the ith and mth cracks, integral point coordinate $t(i)$, and collocation point $t(m)$ in the following way:

$$\psi = \beta - \theta_c^{(i)} \quad (7a)$$

$$\phi = \theta_c^{(m)} - \beta \quad (7b)$$

with β defined as

$$\sin\beta = x_p/r_p \quad (8a)$$

$$\cos\beta = y_p/r_p \quad (8b)$$

and

$$x_p = x_c^{(i)} + t^{(i)}\cos\theta_c^{(i)} \quad (9a)$$

$$y_p = y_c^{(i)} + t^{(i)}\sin\theta_c^{(i)} \quad (9b)$$

$$r_p = \sqrt{x_p^2 + y_p^2}. \quad (9c)$$

Also, the kernels J_{ijk} may be replaced as

$$J_{ijk} = J_{ijk}(t^{(i)}, t^{(m)}) = J_{ijk}(x, y; \xi) \quad (10)$$

with x, y, and ξ found as

$$x = r^{(m)}\cos(\gamma - \beta) + t^{(m)}\cos(\theta_c^{(m)} - \beta) \quad (11a)$$

$$y = r^{(m)}\sin(\gamma - \beta) + t^{(m)}\sin(\theta_c^{(m)} - \beta) \quad (11b)$$

$$c = r_p. \quad (11c)$$

Here, $r(m)$ represents the distance between the origin of the inclusion and the center of the mth crack and γ is the angle between the x-axis and the line connecting the origin and the center of the mth crack.

It may be observed that eqn (5) gives rise to $2M$ integral equations. In order to solve these equations completely for $b_l^{(i)}(l=1,2)$, however, we need to evaluate $2M$ additional constants of integrations. The $2M$ additional equations may be obtained by considering the single valuedness of the displacements. This yields

$$\int_{-a^{(i)}}^{a^{(i)}} b_l^{(i)}(t^{(i)})\,\mathrm{d}t^{(i)} = 0 \quad l=1,2 \tag{12}$$

Equations (5) and (12), together, now provide an integral equation representation of the micro-scale effects containing M interacting micro-cracks around the inclusion in an infinite matrix. These governing integral equations can be solved very accurately and effectively (Hu and Chandra (1993a,b,c)) using the Gauss-Chebychev quadrature scheme proposed by Erdogan *et al.* (1973) for singular integral equations.

The discretized system contains $2M(L-1)$ algebraic equations (where L is the number of Gauss points on a crack and M is the number of cracks) but $2ML$ unknowns. Equation (12), expressing the continuity of crack opening shapes, provides the additional $2M$ equations.

After solving the integral equations (5) and (12), one may get the displacement and stress (hence the traction) fields in the second sub-problem shown in Fig. 2. Knowing $u_i^{(R2)}$ and $\tau_i^{(R2)}$, as well as the unit vectors, the appropriate kernels $\bar{\bar{U}}_{ij}$ and $\bar{\bar{T}}_{ij}$ may now be obtained (Chandra *et al.* (1995), Rizzo (1994)) for use in a macro-scale BEM analysis. These may be expressed as,

$$u_i^{(R2)}(p) = \bar{\bar{U}}_{ij}(p,q)e_j(q) \tag{13a}$$

and

$$t_i^{(R2)}(p) = \bar{\bar{T}}_{ij}(p,q)e_j(q) \tag{13b}$$

for the desired sets of source and field points. The kernels $\bar{\bar{U}}_{ij}$ and $\bar{\bar{T}}_{ij}$ capture the effects due to micro-scale crack-crack as well as crack-inclusion interactions.

The complete augmented kernels may now be constructed as

$$\acute{U}_{ij}(p,q) = U_{ij}(p,q) + \bar{U}_{ij}(p,q) + \bar{\bar{U}}_{ij}(p,q) \tag{14a}$$

and

$$\acute{T}_{ij}(p,q) = T_{ij}(p,q) + \bar{T}_{ij}(p,q) + \bar{\bar{T}}_{ij}(p,q) \tag{14b}$$

where U_{ij} and T_{ij} are the conventional kernels obtained from the Kelvin solution (2); $\bar{U}_{ij}$ and $\bar{T}_{ij}$ are the kernels representing perturbations due to elastic inclusions; $\bar{\bar{U}}_{ij}$ and $\bar{\bar{T}}_{ij}$ are the kernels capturing the effects of the micro-cracks on the particle reinforced composite (details of these kernels are provided in the Appendix). The augmented kernels $\acute{U}_{ij}$ and $\acute{T}_{ij}$, capturing the micro-scale effects, may now be utilized directly in a macro-scale BEM analysis of general elastic structures subject to realistic loadings and boundary conditions.

3. MICRO-MACRO BEM FORMULATION

Using Betti's reciprocal theorem (e.g., Banerjee and Butterfield (1981), Mukherjee (1982), Brebbia and Dominguez (1992)) or a weighed residual approach (Okada *et al.* (1990)), a hybrid BEM formulation requiring only macro-scale discretization may be developed as (Cruse (1988))

$$u_j(p) = \int_{\partial B} [\acute{U}_{ij}(p, Q)\tau_i(Q) - \acute{T}_{ij}(p, Q)u_i(Q)]\, ds_Q. \tag{15}$$

Equation (15) captures the effects of inclusions and micro-cracks through the augmented kernels. A boundary integral equation for the unknown components of displacements and tractions in terms of the prescribed ones can be obtained by taking the limit as the internal source point p approaches a boundary point P. This leads to the boundary equation

$$C_{ij}u_i(P) = \int_{\partial B} [\acute{U}_{ij}(P, Q)\tau_i(Q) - \acute{T}_{ij}(P, Q)u_i(Q)]\, ds_Q. \tag{16}$$

As noted in Section 2, the kernels $\bar{U}_{ij}$ and $\bar{T}_{ij}$ are regular everywhere. Also, the kernels $\bar{\bar{U}}_{ij}$ and $\bar{\bar{T}}_{ij}$ will never be singular for a micro-crack cluster that is completely internal to the body. Hence, the singularity of $\acute{U}_{ij}(P, Q)$ and $\acute{T}_{ij}(P, Q)$ will essentially be contained in $U_{ij}(P, Q)$ and $T_{ij}(P, Q)$, respectively. The coefficients C_{ij} multiplying u_i in the free term arise from the integration of $\acute{T}_{ij}(P, Q)u_i(Q)$. Hence, for two-dimensional problems, $C_{ij} = 1/2\delta_{ij}$ if the boundary ∂B is locally smooth at P. Otherwise, C_{ij} can be evaluated in closed form for two-dimensional problems (Mukherjee (1982)). Alternatively, proper combinations of $C_{ij}(P)$ and $\int_{\partial B}\acute{T}_{ij}(P, P)\, ds_Q$ can be obtained indirectly for general two-dimensional and three-dimensional bodies with sharp corners using rigid body modes (Cruse (1974), Cruse (1988)). In the present work, the indirect approach is used to obtain desired combinations of $C_{ij}(P)$ and $\int_{\partial B}\acute{T}_{ij}(P, P)\, ds_Q$ in terms of the off-diagonal terms. It should be noted here, that eqns (15) and (16) involve boundary integrals only and require discretization only on the macro-scale boundary ∂B of the body. Thus, the traditional advantages of a BEM approach for homogeneous problems (e.g., Banerjee and Butterfield (1981), Mukherjee (1982), Cruse (1988)) are completely preserved.

The next step in the BEM formulation is to obtain the internal stresses. To achieve this goal, eqn (15) is analytically differentiated at an internal source point p:

$$u_{j,\bar{l}}(p) = \int_{\partial B} [\acute{U}_{ij,\bar{l}}(p, Q)\tau_i(Q) - \acute{T}_{ij,\bar{l}}(p, Q)u_i(Q)]\, ds_Q. \tag{17}$$

Here, $\bar{l}$ following a comma denotes differentiation with respect to a source point. The resulting displacement gradients at the source point can then be used in a Hook's law to determine the internal stresses

$$\sigma_{ij} = \lambda u_{k,k}\delta_{ij} + G(u_{i,j} + u_{j,i}). \tag{18}$$

The differentiated kernels $\acute{U}_{ij,\bar{k}}$ and $\acute{T}_{ij,\bar{l}}$ must now be evaluated. These may be written as

$$\acute{U}_{ij,\bar{k}} = U_{ij,\bar{k}} + \bar{U}_{ij,\bar{k}} + \bar{\bar{U}}_{ij,\bar{k}} \tag{19a}$$

and

$$\acute{T}_{ij,\bar{k}} = T_{ij,\bar{k}} + \bar{T}_{ij,\bar{k}} + \bar{\bar{T}}_{ij,\bar{k}}. \tag{19b}$$

Here, $U_{ij,\bar{k}}$ and $T_{ij,\bar{k}}$ are the source point derivatives of U_{ij} and T_{ij}. Since U_{ij} and T_{ij} are two point kernels and

$$U_{ij,\bar{k}} = -U_{ij,\bar{k}}; \quad T_{ij,\bar{k}} = -T_{ij,\bar{k}} \tag{20}$$

these may be evaluated easily using analytical techniques. Similarly, $\bar{U}_{ij,\bar{k}}$ and $\bar{\bar{T}}_{ij,\bar{k}}$ can be determined in closed forms.

The kernels $\bar{\bar{U}}_{ij,\bar{k}}$ and $\bar{\bar{T}}_{ij,\bar{k}}$ depend on the sizes and distributions of the micro-cracks. Hence, they cannot be easily represented in terms of the corresponding field point derivatives. The source point derivatives of displacements may, however, be obtained by directly differentiating the displacement components u_i ($i = 1, 2$) in eqn (4a) at a source point. It is interesting to note that the kernels K_{j11} through K_{j22} in eqn (5) do not depend on the macro-scale source points. Accordingly, the source point displacement and stress gradients may be written as

$$u_{j,\bar{l}}(p) = \frac{1}{2\pi(1-\nu_1)} H_{jk} b_{k,\bar{l}}(p) \tag{21a}$$

$$\sigma_{ij,\bar{l}}(p) = \frac{G_1}{\pi(1+\kappa_1)} J_{ijk} b_{k,\bar{l}}(p). \tag{21b}$$

Here, $b_{k,\bar{l}}$ may be evaluated from direct differentiation of eqn (5) as

$$\sum_{i=1}^{M} \int_{-a^{(i)}}^{a^{(i)}} [K_{jkl}(t^{(m)}, t^{(i)}) b^{(i)}_{l,\bar{m}}(t^{(i)})]\, \mathrm{d}t^{(i)} + \sigma^{(m_0)}_{jk,m}(t^{(m)}) = 0. \tag{22}$$

Again, $K_{jkl}(t^{(m)}, t^{(i)})$ are independent of the macro-scale source points and $\sigma^{(m_0)}_{jk,m}(t^{(m)})$ represents the stress gradient at the location of the mth crack but without any cracks in the system. Accordingly, $b_{l,\bar{m}}$ can easily be evaluated by solving eqn (22).

For efficient computations, eqn (22) can actually be solved by retaining the same matrix decompositions used for solving eqn (5) and modifying the right-hand side. Then, $u_{j,\bar{l}}(p)$ may be obtained from eqn (21a). The augmented kernels $\hat{U}_{ij,\bar{l}}$ and $\hat{T}_{ij,\bar{l}}$ may then be obtained from eqn (18). The stresses at an internal point may now be evaluated through eqns (17)–(18).

In order to evaluate the stress intensity factors (SIF) at the crack tip, the stresses are evaluated at several points near the crack tip and the SIF is interpolated. It has been observed by Owen and Fawkes (1983) that stress evaluations at $0.01a$, $0.04a$, and $0.16a$ (a being the half-length of the crack) are optimum for this purpose. Chandra *et al.* (1995) found the stress evaluation at $0.01a$ can also give very good SIF results but with better efficiency. A similar scheme is used here to determine the crack tip SIFs. An alternative scheme involving only boundary quantities, recently proposed by Huang *et al.* (1995), may also be used for determining crack opening displacements and crack tip SIFs. The scheme is based on the reciprecal theorem in order to evaluate the crack opening and sliding displacements near each crack tip.

The computation of the boundary stresses may be carried out following well established techniques (e.g., Cruse and Vanburen (1971), Rizzo and Shippy (1977), Chandra and Mukherjee (1984, 1987)).

For two-dimensional problems, the calculation involves four vectors and two tensors at the source point P on the boundary. The vectors are tractions τ_i, the tangential derivative of displacement $\partial u_i/\partial t$ on ∂B at P, as well as the unit normal and tangent vectors n and t at P. The tensors are the stresses σ_{ij} and displacement gradients $u_{j,\bar{l}}(p)$. The 7 unknown tensor components, σ_{ij} and $u_{j,\bar{l}}(p)$, can now be obtained from the following set of equations (7 scalar linear algebraic equations) at P:

$$\sigma_{ij} = \lambda u_{k,k}\delta_{ij} + G(u_{i,j} + u_{j,i}) \tag{23a}$$

$$\tau_i = \sigma_{ji} n_j \tag{23b}$$

$$\frac{\partial u_i}{\partial t} = u_{i,j} t_j. \tag{23c}$$

In eqn (23c), the tangential gradients of displacement ($\partial u_i/\partial t$) need to be evaluated numerically from the known boundary displacements. The tractions (τ_i) are also known, and eqn

(23) involving 7 unknowns in σ_{ij} and $u_{i,j}$ can be solved from 7 scalar linear algebraic equations.

4. NUMERICAL IMPLEMENTATIONS

Numerical implementations of the BEM eqns (15)–(17) for analyzing planar elastic problems containing circular inclusions and multiple cracks are considered in this section. The boundary of the macro-scale problem is divided into N boundary segments (or elements). Geometric corners are accounted for through zero-length elements (Mukherjee (1982)). Suitable shape functions must be chosen for the variations of displacements and tractions on the boundary elements. In the present work, straight boundary elements are used with linear shape functions for both displacements and tractions. No other discretization is necessary for the macro-scale problem, and the micro-scale effects of the inclusion and micro-cracks are introduced through the augmented fundamental solutions.

For the micro-scale problem, 9 integration points are used on each crack for solving eqn (5). A Gauss-Chebychev polynomial scheme requires only n quadrature points for accurate representations of polynomial functions of order $2n$. This makes it very effective for interacting inclusions and cracks at close spacings. The issues regarding the effectiveness of such a scheme are available in various references (e.g., Erdogan (1975), Theocaris and loakimidis (1977), Melin (1983), Li and Hills (1990), Rubinstein (1990), Hu and Chandra (1993a,b), and Chandra *et al.* (1995)).

All integrations involving kernels U_{ij} and T_{ij} are carried out analytically, and all integrations regarding kernels $\bar{U}_{ij}$ and $\bar{T}_{ij}$ are obtained by standard Gauss quadrature. The kernels $\bar{\bar{U}}_{ij}$ and $\bar{\bar{T}}_{ij}$ are found numerically. Accordingly, all integrations involving these kernels are also carried out numerically. It is interesting to note here, that the kernels $\bar{U}_{ij}$ and $\bar{T}_{ij}$ as well as $\bar{\bar{U}}_{ij}$ and $\bar{\bar{T}}_{ij}$ are regular while the source point lies on the boundary. Hence, the accuracy of the proposed BEM scheme is not compromised by the numerical integration of these kernels.

Finally, the boundary eqn (16) may be transformed into an algebraic system of the type

$$[A]\{u\} + [B]\{\tau\} = 0 \tag{24}$$

for the complete elastic micro-macro problem. In eqn (24), only macro-scale discretizations are needed and the micro-scale effects are incorporated through the augmented fundamental solution (14). Equation (24) may now be solved easily for unknown displacements and tractions for a well-posed problem. For the square macro-scale domains used in example problems a total of 44 boundary nodes with 40 boundary elements are used. Another two sets of numerical computations were carried out with 64 boundary nodes and 60 boundary elements, and 124 nodes and 120 elements, respectively. For the specific problem configuration shown in Fig. 5, the normalized mode I SIF(K_I) differed by less than 0.25% as number of boundary elements were increased from 40 to 120, showing convergence of numerical results.

5. NUMERICAL RESULTS

The proposed hybrid micro-macro BEM scheme is first verified against known solutions involving inclusion-crack interactions. For all cases, the stress intensity factors are normalized with respect to that for a single crack in an infinite plane ($\sigma_0\sqrt{\pi a}$ for uniaxial, and $\tau_0\sqrt{\pi a}$ for pure shear loading), where σ_0, τ_0 are the remote stresses and a is the half length of the crack. In this section, the radius of the inclusion is denoted as R. The proposed BEM scheme can handle plane stress or plane strain problems, however, only plane strain problems are considered in this section.

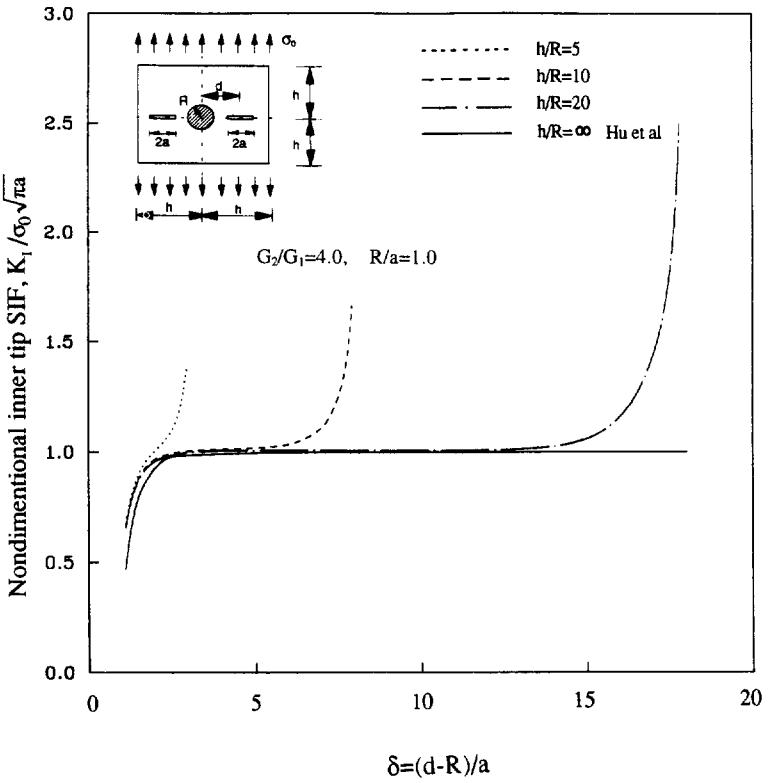

Fig. 3. Effect of inclusion size parameter h/R on the normalized SIF for harder inclusions vs the normalized geometry parameter δ.

As shown in the inset of Fig. 3, a problem with a circular inclusion of radius R at the center of a square (of dimension $2h \times 2h$) finite domain and accompanied by two collinear symmetric cracks of length $2a$ each is considered first. The square domain is subjected to uniaxial tension. The distance of the center of the crack from the center of the inclusion is denoted by d. Accordingly, the non-dimensional parameter $\delta = (d\text{-}R)/a$ represents the proximity of the cracks to the inclusion or the boundary of the domain. The ratio h/R represents the size of the square domain relative to the inclusion. The normalized mode-*I* SIFs at the inner crack tips obtained from the hybrid micro-macro BEM computations at different h/R values of 5, 10 and 20 are plotted in Fig. 3 with respect to δ. Harder inclusions with $G_2/G_1 = 4.0$ and $\nu_2 = \nu_1 = 0.25$ are used in these computations. It may be observed from Fig. 3 that the results compare very well to those obtained by Hu *et al.* (1993c) for $h/R = \infty$, when the boundary of the domain remains far away from the micro-features. Significant deviations in mode-*I* SIFs are observed as the micro-features approach and interact with the boundary. Figure 4 depicts the same situation as that in Fig. 3, but with a softer inclusion ($G_2/G_1 = 0.25$). It is observed that the crack-inclusion interactions are very strong at close spacings. When the micro-features remain far away from the edge of the body, the mode-*I* SIFs for softer inclusions also agree very well with those obtained by Hu *et al.* (1993c) for $h/R = \infty$. As the cracks move toward the edges of the square body, inclusion-crack interactions become weaker while the edge-crack interactions become stronger.

Figure 5 shows the effects of variations in material properties of the inclusion relative to the matrix material on the inner-tip SIFs. The effects of variations in shear modulus are shown in Fig. 5 for $h/R = 20$ and $\nu_1 = \nu_2 = 0.25$. The ratio of the shear moduli is varied as $G_2/G_1 = 4.0$, 1.0 and 0.25, respectively. It is observed that such variations produce significant effects only at close spacings to interacting cracks. It is well known that the interactions of collinear cracks in a homogeneous solid always produce amplifications of the inner-tip SIFs. It can be clearly seen in Fig. 5 that the presence of an inclusion between the collinear cracks significantly affect the SIFs at the crack tips. A softer inclusion amplifies the SIFs,

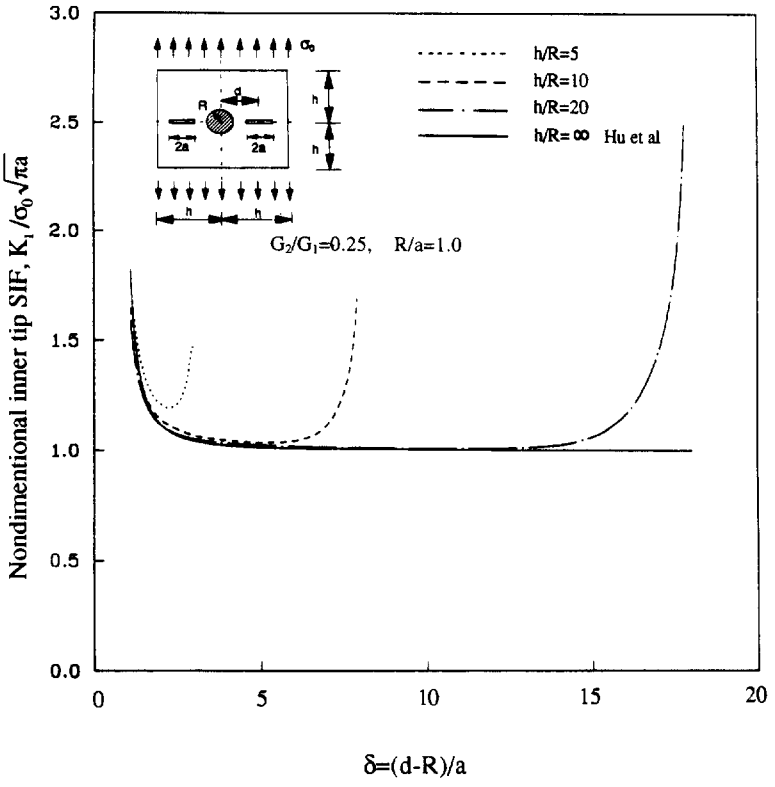

Fig. 4. Effect of inclusion size parameter h/R on the normalized SIF for softer inclusions vs the normalized geometry parameter δ.

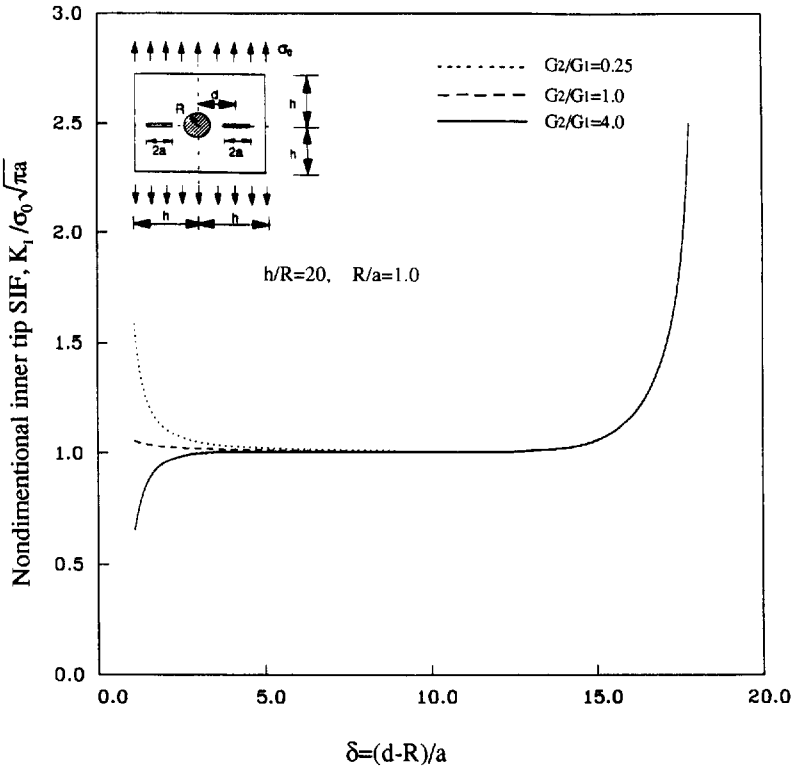

Fig. 5. Effect of matrix-inclusion stiffness ratio on the normalized SIF vs the normalized geometry parameter δ.

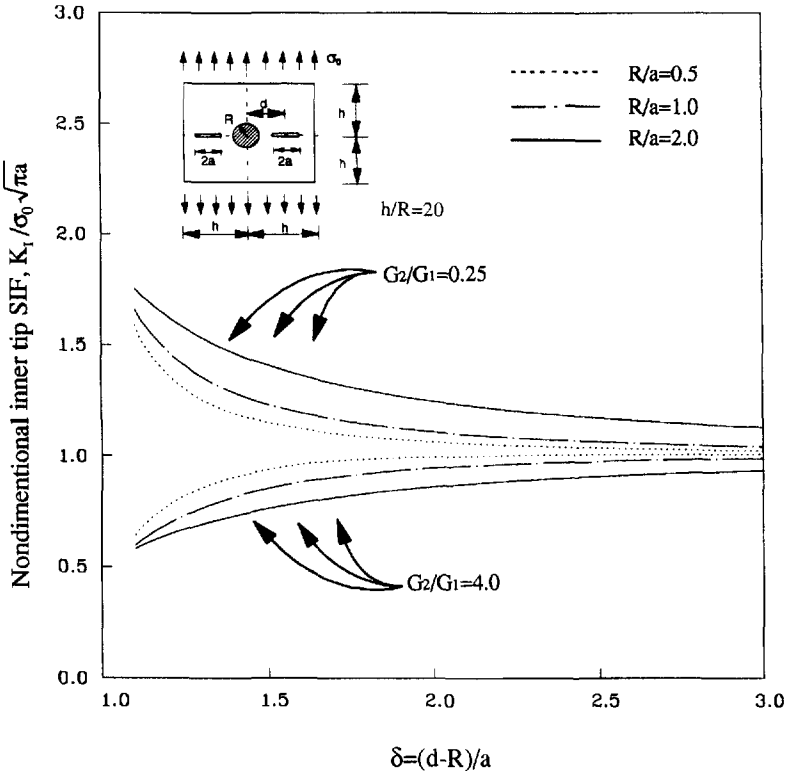

Fig. 6. Effect of the ratio R/a on the normalized SIF vs the normalized geometry parameter δ.

while a harder inclusion provides shielding. Variations in Poisson's ratio v_2/v_1 also produce similar effects as that due to variations in shear modulus ratio G_2/G_1. However, such effects due to variations in v_2/v_1 have been observed to be less significant than the SIF modulations induced by variations in G_2/G_1.

The effects due to variations in relative sizes of inclusions compared to cracks (denoted by R/a ratio) are investigated next. Figure 6 shows the SIF modulations at varying $\delta = (d-R)/a$, for three different R/a ratios = 0.5, 1 and 2, for both harder ($G_2/G_1 = 4.0$) and softer ($G_2/G_1 = 0.25$) inclusions. As expected, harder inclusions produce stress shielding, while softer inclusions lead to stress amplifications. The SIF modulations are greatest at smaller values of δ. At a fixed δ, a greater R/a ratio produces a higher modulation. For example, at $\delta = 1.5$, SIF changes from 0.9377 to 0.7611 (for $G_2/G_1 = 4.0$), and 1.1489 to 1.4066 (for $G_2/G_1 = 0.25$), as R/a is varied from 0.5 to 2.

A square domain containing an inclusion surrounded by a varying number of radial cracks and subjected to uniaxial tension is investigated next. Such radial cracking may commonly occur from secondary phases due to mismatch in coefficients of thermal expansion (Huang *et al.*, (1992)) and associated transformation loadings. The number of radial cracks is varied from 2 to 8 with equal spacing. The inner SIF values are taken from the horizontally oriented cracks. As observed in Fig. 7, a hard inclusion ($G_2/G_1 = 4.0$, $v_1 = v_2 = 0.25$) provides shielding in general. This shielding, however, is tempered by crack-crack interactions that become stronger as the number of radial cracks increases and their spacing decreases. It is interesting to note, however, that the SIF modulations due to such interactions are nonlinear in nature. As N (number of cracks) is changed from 2 to 4, the SIF modulation is negligible. However, it becomes much more significant as N is increased further to 4 and 8. Such effects may be explained by the fact that, at closer spacings, the radial cracks also provide shielding due to crack-crack interactions. Accordingly, the overall shielding is stronger at higher number of radial cracks. At $\delta = 1.1$, the normalized SIF drops from 0.5977 at $N = 4$ to 0.3092 for $N = 8$. Figure 8 shows the SIFs for the same

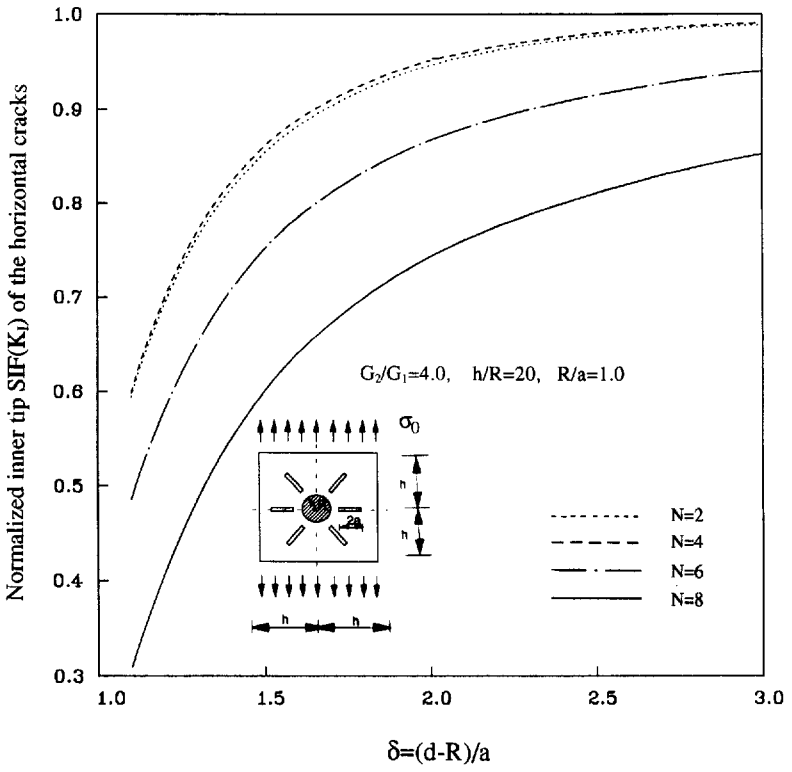

Fig. 7. Effect of the crack number on the normalized inner tip SIF(K_I) of the horizontal cracks vs the normalized δ.

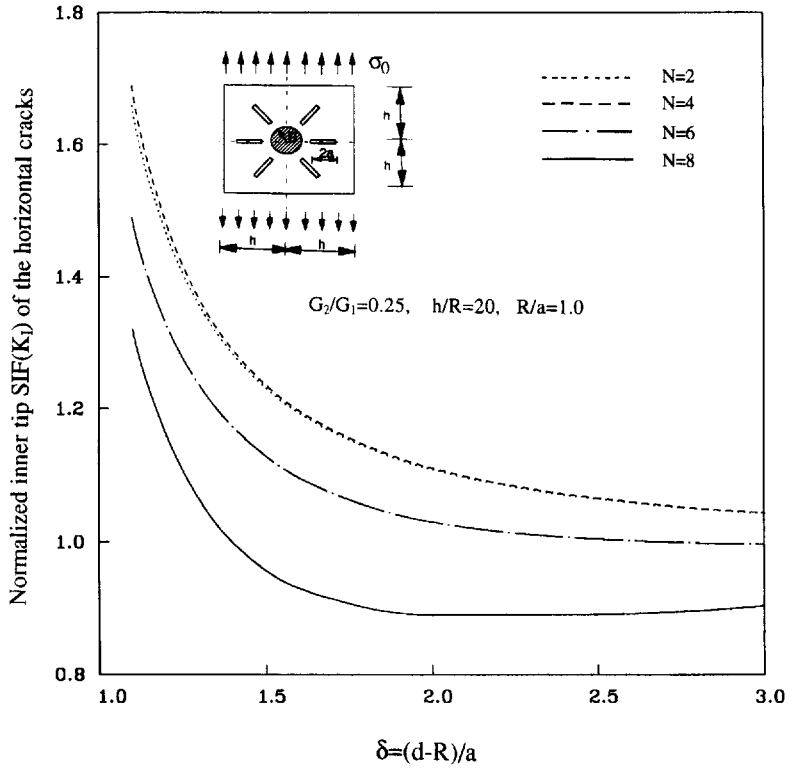

Fig. 8. Effect of the crack number on the normalized inner tip SIF(K_I) of the horizontal cracks vs the normalized δ.

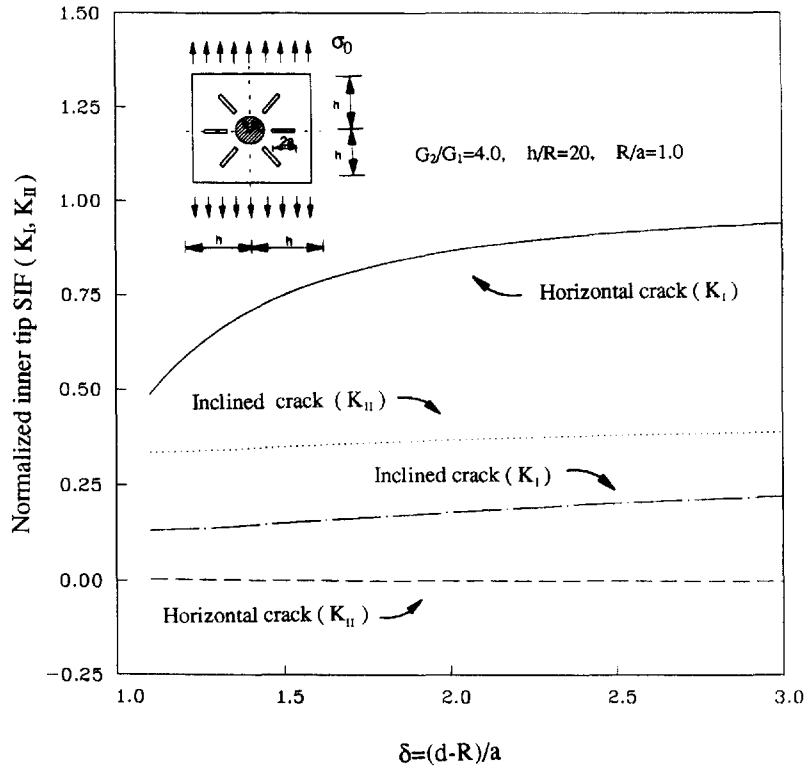

Fig. 9. Variation of the normalized SIF(K_I, K_{II}) of the inclined and horizontal cracks close to a harder inclusion vs the normalized geometry parameter δ.

problem but with a softer inclusion ($G_2/G_1 = 0.25$). A softer inclusion causes stress amplification, in general, due to inclusion-crack interactions. However, as the number of radial cracks increases (>4), this amplification is modulated by the shielding effects due to crack-crack interactions among radial cracks. It may be observed from Fig. 8 that, at $\delta = 1.1$, the normalized inner-tip SIF drops from 1.69 for $N = 4$ to 1.3216 for $N = 8$. It is also observed that, depending on the number of radial cracks, the softness of the inclusion and their spacings, there exists a critical number of radial cracks, above which the overall behavior manifested by the normalized SIFs may change from amplification to shielding (e.g., $G_2/G_1 = 0.25$, $R/a = 1.0$, $N = 8$, $\delta > 1.4$). Comparisons of mode *I* and mode *II* SIFs for $R/a = 1.0$, $h/R = 20$ and $N = 6$ are shown in Fig. 9 (harder inclusion: $G_2/G_1 = 4.0$) and Fig. 10 (softer inclusion: $G_2/G_1 = 0.25$). K_I and K_{II} for the horizonatal crack along the positive x-axis and the inclined crack in the first quadrant are shown. As expected, K_{II} for the horizontal crack is zero under uniform uniaxial loading in the vertical direction. The inclined crack exhibits non-zero K_I and K_{II}. Due to the high mode *I* SIF, however, the horizontal crack will be expected to propagate first. With increasing δ, this K_I increases for the harder inclusion, but decreases for the softer inclusion. In both cases, the K_I approaches an asymptotic value of 1.0 for large δ. For very large δ, however, the outer crack tip would interact with the free edge of the plate (as shown in Figs 3 and 4), and K_I would increase again.

Finally, the problem of a circular inclusion accompanied by two collinear cracks in a square finite body under pure shear loading is considered. In this case, $h/R = 20$, material properties are taken as $\nu_1 = \nu_2 = 0.25$ and $G_2/G_1 = 4.0$. Under pure shear loading, the computations show that the dominant term is K_{II} while K_I is very small and negligible. As shown in Fig. 11, similar to uniaxial loading, the crack-inclusion interactions provide shielding to the K_{II}s. Hu *et al.* (1993c), have obtained SIFs for infinite bodies, that are valid when cracks are far away from the edge of the finite domain. For $h/R = 20$, the BEM results compare very well to those obtained by Hu *et al.* (1993c) for an infinite body.

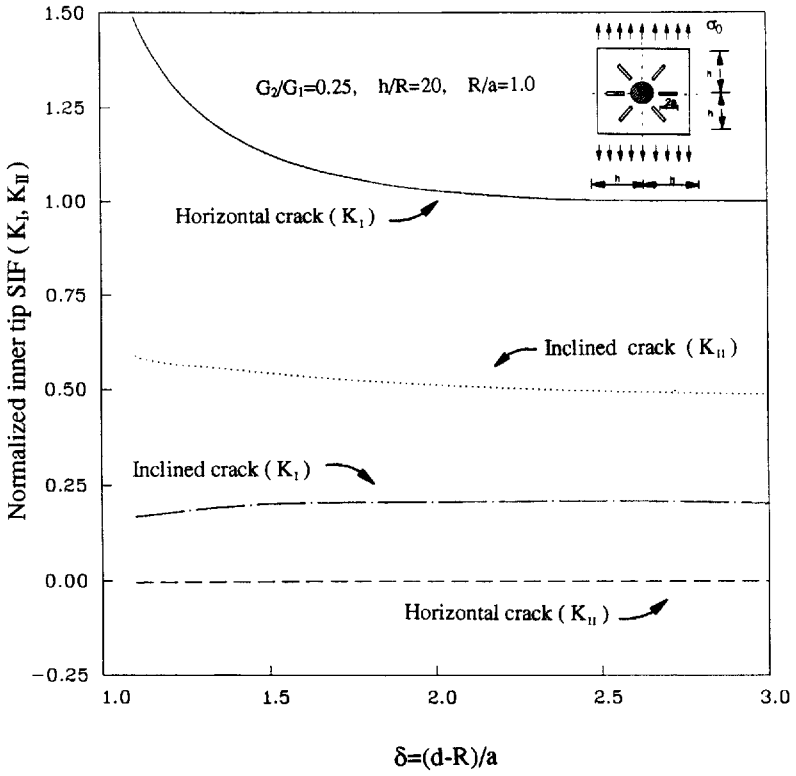

Fig. 10. Variation of the normalized SIF(K_I, K_{II}) of the inclined and horizontal cracks close to a softer inclusion vs the normalized geometry parameter δ.

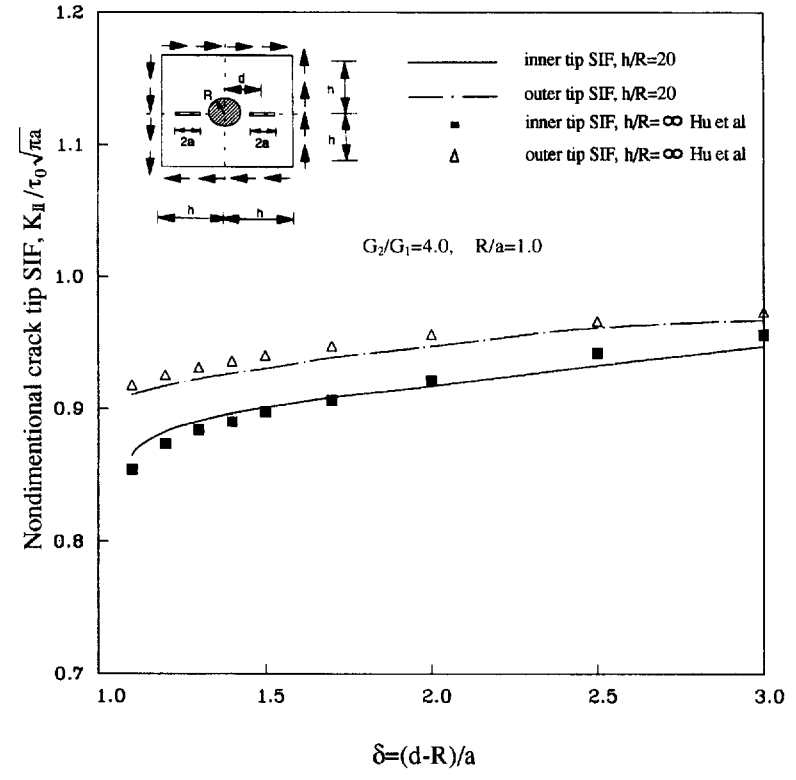

Fig. 11. Variation of the normalized SIF(K_{II}) vs parameter δ.

6. DISCUSSION AND SUMMARY

The problem of interacting micro-cracks around an inclusion in a system involving complex finite geometries and general boundary conditions is considered in this paper. A hybrid micro-macro BEM formulation capable of handling interactions among the inclusion, arbitrarily distributed cracks and the boundaries of the system is developed. The effects of micro-scale features are introduced into the macro-scale BEM analysis through an augmented fundamental solution. Thus, the hybrid scheme retains the boundary nature of the problem and associated advantages of a BEM formulation.

Several numerical examples have been shown in order to verify and validate the capability of the proposed BEM formulation for analyzing problems stated above. It is observed that the proposed scheme can solve these problems accurately and effectively. The numerical results reveal that the inclusion-crack and crack-crack interactions can greatly affect the nature of local stress distributions.

Many real-life materials are reinforced as matrix materials by mixing some fibers to form composite materials. During the processing and later routine use of these composite materials, it is quite likely that some micro-cracks would nucleate around the fibers. The proposed hybrid micro-macro BEM formulation can capture the effects of such micro-scale phenomena within the context of macro-scale structural computations. The proposed technique can also be generalized through a unit cell approach to obtain effective macro-scale material properties based on its micro-scale features (Huang *et al.* (1995)).

Acknowledgement—The authors gratefully acknowledge the financial support furnished by grant No. CMS 9522147 from the U.S. National Science Foundation.

REFERENCES

Atkinson, C. (1972). The Interaction between a crack and an inclusion. *Int. J. Engng Sci.* **10,** 127–136

Banerjee, P. K. and Butterfield, R. (1981). *Boundary Element Method in Engineering Science*. McGraw-Hill, London.

Banerjee, P. K. and Henry, D. P. (1992). Nonlinear Micro and Macromechanical Analyses of Composites by BEM. In *Proc., HITEMP Conference*, Vol. 2, NASA Lewis Res. Center, Cleveland, pp. 42.1–42.11.

Barsoum, R. S. (1976). On the use of isoparametric finite elements in linear fracture mechanics. *Int. J. Num. Meth. Engng* **10,** 25–27.

Bathe, K. J., (1982). *Finite Element Procedures in Engineering Analysis*, Prentice-Hall, Englewood Cliffs, N.J.

Becker, R. (1992). An Analysis of Shear Localization During Bending of a Polycrystalline sheet. *ASME J. Appl. Mech.* **59,** 491–496.

Becker, P., Hsueh, C.-H., Angelini, P. and Tiegs, T. N. (1988). Toughening behavior in whisker-reinforced ceramic matrix composites. *J. Am. Ceramic. Soc.* **71,** 1056–1061.

Bibly, B. A. and J. D. Eshelby (1968). Dislocation and the theory of fracture. In *Fracture*; *An Advanced Treatise*, Vol. 1 (ed. H. Leibowitz), Academic Press, New York, pp. 99–182.

Brebbia, C. A. and J. Dominguez (1989). *Boundary Elements: An Introductory Course*. Boston Publishers, Southampton.

Budiansky, B. (1965). On the elastic moduli of some heterogeneous material. *J. Mech. Phys. Solids* **13,** 223–227.

Chandra, A. and Mukherjee, S. (1984). Boundary element formulations for large strain-large deformation problems of viscoplasticity. *Int. J. Solids and Struct.* **20,** 41–53.

Chandra, A. and Mukherjee, S. (1987). A boundary element analysis of metal extrusion processes. *ASME, J. App. Mech.* **54,** 335–340.

Chandra, A. and Mukherjee, S. (1995). *Boundary Element Methods in Manufacturing*, Oxford University Press, New York (in press).

Chandra, A. and Tvergaard, V. (1993). Void nucleation and growth during plane strain exclusion. *Int. J. Damage Mech.* **2,** 330–348.

Chandra, A., Huang, Y., Wei, X. and Hu, K. X. (1995). A hybrid micro-macro BEM formulation for micro-crack clusters in elastic components. *Int. J. Num. Meth. Engng* **38,** 1215–1236.

Christensen, R. M. and Lo, K. H. (1979). Solutions for effective shear properties in three phase sphere and cylinder models. *J. Mech. Phys. Solids* **27,** 315–330.

Crouch, S. L. (1976). Solution of plane elasticity problems by the displacement discontinuity method. *Int. J. Num. Meth. Engng* **10,** 301–343.

Cruse, T. A. (1974). An improved boundary-integral equation method for three-dimensional elastic stress analysis. *Computers and Structures* **4,** 741–754.

Cruse, T. A. (1988). *Boundary Element Analysis in Computational Fracture Mechanics*, Kluwer Academic Publishers, Dordrecht, The Netherlands.

Cruse, T. A. and Polch, E. Z. (1986). Application of an elastoplastic boundary element method to some fracture mechanics problems. *Engng Fract. Mech.* **23,** 1085–1096.

Dundurs, J. and Markenscoff, X. (1989). A Green's function formulation of anticracks and their interaction with load induced singularities. *J. Appl. Mech.* **56,** 550–555.

Dundurs, J. and Mura, T. (1964). Interaction between an edge dislocation and a circular inclusion. *J. Mech. Phys. Solids* **12,** 177–189.
Dundurs, J. and Sendeckyj, G. P. (1965). Edge dislocation inside a circular inclusion. *J. Mech. Phys. Solids* **13,** 141–147.
Erdogan, F. (1962). On the stress distribution on plates with collinear cuts under arbitrary loads. In *Proc. 4th U.S. National Congress of Applied Mechanics*, ASME, New York pp. 547–553.
Erdogan, F., Gupta, G. D. and Cook, T. S. (1973). Numerical solution of singular integral equations. In *Methods of Analysis and Solutions of Crack Problems* (ed. G. C. Sih), Noordhoff, Leyden, The Netherlands, pp. 386–425.
Fleck, N. A., Hutchinson, J. W. and Tvergaard, V. (1989). Softening by void nucleation and growth in tension and shear. *J. Mech. Phys. Solids* **37,** 515–540.
Gallagher, R. H. (1975). *Finite Element Analysis: Fundamentals*, Prentice-hall, Englewood Cliffs, N.J.
Hill, R. (1965). A self-consistent mechanics of composite materials. *J. Mech. Phys. Solids* **13,** 213–222.
Horii, H. and Nemat-Nasser, S. (1986). Brittle failure in compression: splitting, faulting and brittle-ductile transition. *Phil. Trans. Royal Soc. Lond.* **A319,** 337–374.
Hu, K. X. and Chandra, A. (1993a). Interactions among general systems of cracks and anticracks: an integral equation approach. *ASME J. Appl. Mech.*, **60,** 920–928.
Hu, K. X. and Chandra, A. (1993b). Interactions among cracks and rigid lines near a free surface. *Int. J. Sol. Struct.* **30,** 1919–1937.
Hu, K. X., and Chandra, A., and Huang, Y. (1993c). Fundamental solutions for dilute distributions of inclusions embedded in microcracked solids. *Mech. Mater.* **16,** 281–294.
Hu, K. X., Chandra, A., and Huang, Y. (1994). On interacting bridged crack systems. *Int. J. Sol. Struc.* **31,** 599–611.
Huang, Q. and Cruse, T. A. (1994). On the nonsingular traction-BIE in elasticity. *Int. J. Num. Meth. Engng* **37,** 2041–2062.
Huang, Y., Hu, K. X., Wei, X., and Chandra, A. (1994). A generalized self-consistent mechanics method for composite materials with multiphase inclusions. *J. Mech. Phys. Solids* **42,** 491–504.
Huang, Y., K. X. Hu and A. Chandra (1995). Stiffness evaluation for solids containing dilute distributions of inclusions and microcracks. *J. Appl. Mech.* **62,** 71–77.
Huang, Y., Chandra, A., Jiang, Z. Q., Wei, X. and Hu, K. X. (1995). The numerical calculation of two-dimensional effective moduli for microcracked solids. *Int. J. Solids. Struct.* (in press).
Hughes, T. J. R. (1987). *The Finite Element Method*, Prentice-Hall, Englewood Cliffs, N.J.
Kamel, M. and Liaw, B. M. (1991a). Boundary element analysis of cracks at a fastner hole in an anisotropic sheet. *Int. J. Fract.* **50,** 263–280.
Kamel, M. and Liaw, B. M. (1991b). Boundary element formulation with special kernels for an anisotropic plate containing an elliptical hole or a crack. *Engng Fract. Mech.* **39,** 695–711.
Lachat, J. C. (1975). A further development of the boundary-integral technique for elastostatics. Ph. D. thesis, University of Southampton, England.
Li, Y. and Hills, D. A. (1990). Stress intensity factor solutions for kinked surface cracks. *J. Strain Analysis* **25,** 21–27.
Liu, N. and Altiero, N. J. (1991). Multiple cracks and branch cracks in finite plane bodies. *Mech. Res. Com.* **18,** 233–244.
Lutz, E., Ingraffea, A. R. and Gray, L. J. (1992). Use of simple solutions for boundary integral methods in elasticity and fracture analysis. *Int. J. Num. Meth. Engng* **35,** 1737–1752.
Melin, S. (1983). Why do cracks avoid each other. *Int. J. Fracture* **23,** 37–45.
Mukherjee, S. (1982). *Boundary Element Methods in Creep and Fracture*, Elsevier Applied Science, London.
Nakamura, T. and Suresh, S. (1993). Effects of thermal residual stresses and fiber packing on deformation of metal-matrix composites. *Acta Metall. Mater.* **41,** 1665–1681.
Needleman, A. (1987). A continuum model for void nucleation by inclusion debonding. *ASME J. Appl. Mech.* **54,** 525–531.
Needleman, A. and Tvergaard, V. (1991). A numerical study of void distribution effects on dynamic ductile crack growth. *Engng Fract. Mech.* **38,** 157–173.
Norris, A. N. (1985). A differential scheme for the effective moduli of composites. *Mech. of Materials* **4,** 1–16.
Oden, J. T. (1972). *Finite Elements of Nonlinear Continua*, McGraw-Hill, New York.
Okada, H., Rajiyah, H., and Atluri, S. N. (1990). A full tangent stiffness field-boundary element formulation for geometric and material nonlinear problems of solid mechanics. *Int. J. Num. Meth. Eng.* **29,** 15–35.
Owen, D. R. J. and Fawkes, A. J. (1983). *Engineering Fracture Mechanics: Numerical Methods and Applications*, Pineridge Press, Swansea, U.K.
Raveendra, S. T. and Banerjee, P. K. (1992). Boundary element analysis of cracks in thermally stressed planar structures. *Int. J. Sol. Struct.* **29,** 2301–2317.
Rizzo, F. J. and Shippy, D. J. (1977). An advanced boundary integral equation method for three-dimensional thermoelasticity. *Int. J. Num. Meth. Engng* **11,** 1753–1768.
Rizzo, F. J. (1994). Decomposition of Green's function. Private communication.
Roscoe, R. (1952). The viscosity of suspensions of rigid spheres. *Br. J. Appl. Phys.* **3,** 267–269.
Rubinstein, A. (1990). Crack-path effect on material toughness. *J. Appl. Mech.* **57,** 97–103.
Tada, H., Paris, P. C., and Irwin, G. R. (1985). *The Stress Analysis of Cracks Handbook*. Paris Productions, St Louis, Missouri.
Taya, M. and Chou, T.-W. (1981). On two kinds of ellipsoidal inhomogeneities in an infinite elastic body: an application to a hybrid composite. *Int. J. Solids Struct.* **17,** 553–563.
Theocaris, P. S. and Ioakimidis, N. I. (1977). Numerical integration methods for the solution of singular integral equations. *Quart. Appl. Math.* **35,** 173–182.
Tvergaard, V. (1982). Material failure by void coalescence in localized shear bands. *Int. J. Solids Struct.* **18,** 659–672.
Tvergaard, V. (1989a). Material failure by void growth to coalescence. In *Advances in Applied Mechanics* **27,** Academic Press, San Diego, pp. 83–151.

Tvergaard, V. (1989b). Numerical study of location in a void sheet. *Int. J. Solids Struct.* **25,** 1143–1156.
Tvergaard V. (1990). Effect of fiber debonding in whisker-reinforced metal. *Mater. Sci. Engng A*, **A125,** 203–213.
Weng, G. J. (1984). Some elastic properties of reinforced solids, with special reference to isotropic containing spherical inclusions. *Int. J. Engng Sci.* **22,** 845–856.
Yahia, N. A. B. and Shephard, M. S. (1985). On the effect of quarter-point element size on fracture criteria. *Int. J. Num. Meth. Engng* **20,** 1629–1641.
Zienkiewicz, O. C. and Taylor, R. L. (1991). *The Finite Element Method*, Vol. 2, McGraw-Hill, Berkshire, U.K.

APPENDIX

The perturbation parts $\bar{U}_{ij}$ in eqn (1a) can be derived from the Airy stress functions given by Dundurs and Hetenyi (1961, 1962).

$$\bar{U}_{11}(x,y;\xi)=\frac{1}{4\pi G_1(1+\kappa_1)}\left\{-\frac{A(\kappa_1-1)(\beta^2-1)R}{\beta}\cdot\frac{x_2}{r_2^2}+(A\kappa_1^2+B)(\mathrm{Log}(r)-\mathrm{Log}(r_2))\right.$$
$$-2A\kappa_1\left(\frac{x^2}{r^2}-\frac{x_2^2}{r_2^2}\right)+\frac{A(\beta^2-1)R}{\beta^3}\left[-(\kappa_1+1)\frac{x_2}{r_2^2}+\frac{4x_2^3}{r_2^4}+\frac{(\beta^2-1)R}{\beta}\cdot\left(\frac{1}{r_2^2}-\frac{2x_2^2}{r_2^4}\right)\right]$$
$$\left.+[1+A((\kappa_1-1)\beta^2+1\}-C(\kappa_2+1)]\frac{R}{\beta}\cdot\frac{x}{r^2}+A\kappa_1R^2\left(-\frac{1}{r^2}+\frac{2x^2}{r^4}\right)\right\}$$

$$\bar{U}_{21}=\frac{1}{4\pi G_1(1+\kappa_1)}\left\{-\frac{A(\kappa_1-1)(\beta^2-1)R}{\beta}\cdot\frac{y}{r_2^2}+(A\kappa_1^2-B)(\theta-\theta_2)-2A\kappa_1y\left(\frac{x}{r^2}-\frac{x_2}{r_2^2}\right)\right.$$
$$+\frac{A(\beta^2-1)R}{\beta^3}\left[-(\kappa_1+1)\frac{y}{r_2^2}+\frac{4x_2y}{r_2^4}-\frac{(\beta^2-1)R}{\beta}\cdot\frac{2x_2y}{r_2^4}\right]$$
$$\left.+[1+A((\kappa_1-1)\beta^2+1\}-C(\kappa_2+1)]\frac{R}{\beta}\cdot\frac{y}{r^2}+2A\kappa_1R^2\frac{xy}{r^4}\right\}$$

$$\bar{U}_{12}=\frac{1}{4\pi G_1(1+\kappa_1)}\left\{(A\kappa_1^2-B)(\theta_2-\theta)+2A\kappa_1y\left(\frac{x_2}{r^2}-\frac{x}{r_2^2}\right)-A\frac{(\kappa_1+1)(\beta^2-1)R}{\beta}\frac{y}{r_2^2}\right.$$
$$-\frac{A(\beta^2-1)R}{\beta^3}\left[(\kappa_1-1)\frac{y}{r_2^2}+\frac{4x_2y}{r_2^4}-\frac{(\beta^2-1)R}{\beta}\cdot\frac{2x_2y}{r_2^4}\right]+\left[A((\kappa_1+1)\beta^2-1\}+B\right]\frac{R}{\beta}\cdot\frac{y}{r^2}+A\kappa_1R^2\frac{2xy}{r^4}\Big\}$$

$$\bar{U}_{22}=\frac{1}{4\pi G_1(1+\kappa_1)}\left\{(A\kappa_1^2+B)(\mathrm{Log}(r)-\mathrm{Log}(r_2))+2A\kappa_1\left(\frac{x^2}{r^2}-\frac{x_2^2}{r_2^2}\right)+A\frac{(\kappa_1+1)(\beta^2-1)}{\beta}\right.$$
$$\cdot\frac{Rx_2}{r_2^2}-\frac{A(\beta^2-1)R}{\beta^3}\left[(\kappa_1+3)\frac{x_2}{r_2^2}+\frac{4x_2^3}{r_2^4}-\frac{(\beta^2-1)R}{\beta}\cdot\left(\frac{1}{r_2^2}-\frac{2x_2^2}{r_2^4}\right)\right]$$
$$\left.+[A((\kappa_1+1)\beta^2-1\}+B]\frac{R}{\beta}\cdot\frac{y}{r^2}+A\kappa_1R^2\frac{2xy}{r^4}\right\}.$$

The kernels H_{ij} in eqn (4a) are given as follows:

$$H_{11}(x,y;\xi)=(1+\kappa_1)\cdot\theta_1+2\frac{x_1y}{r_1^2}+(A\kappa_1+B)\cdot(\theta-\theta_2)-\frac{(A-B)}{\beta}\cdot\frac{R\cdot y}{r^2}+2A\cdot y\left(\frac{x}{r^2}-\frac{x_2}{r_2^2}\right)$$
$$-\frac{A(\beta^2-1)\cdot R}{\beta^3}\left(\frac{(\kappa_1-1)\cdot y}{r_2^2}-\frac{2(\beta^2-1)R\cdot x_2\cdot y}{\beta\cdot r_2^4}+\frac{4x_2^2y}{r_2^4}\right)$$

$$H_{21}=(1-\kappa_1)\cdot\mathrm{Log}(r_1)-2\frac{x_1^2}{r_1^2}+(B-A\kappa_1)\cdot(\mathrm{Log}(r)-\mathrm{Log}(r_2))+\frac{(A-B)}{\beta}\cdot\frac{R\cdot x}{r^2}+2A\frac{x_2^2}{r_2^2}$$
$$-\frac{A(2x^2+R^2)}{r^2}-\frac{A(\beta^2-1)\cdot R}{\beta^3}\left((\kappa_1+3)\cdot\frac{x_2}{r_2^2}-\frac{4x_2^3}{r_2^4}-\frac{2(\beta^2-1)R}{\beta}\left(\frac{1}{r_2^2}-\frac{2x_2^2}{r_2^4}\right)\right)+\frac{2AR^2x^2}{r^4}$$

$$H_{12} = -(1-\kappa_1)\cdot \mathrm{Log}(r_1) - 2\frac{x_1^2}{r_1^2} - (B-A\kappa_1)\cdot(\mathrm{Log}(r) - \mathrm{Log}(r_2)) - \frac{2R\cdot x^2}{r^2} + 2A\frac{x_2^2}{r_2^2}$$
$$+ \frac{A(\beta^2-1)\cdot R}{\beta^3}\left(-2\beta\frac{y}{r_2^2} + \frac{(\kappa_1+1)\cdot y}{r_2^2} - \frac{4x_2^2 y}{r_2^4} + \frac{2(\beta^2-1)R\cdot x_2\cdot y}{\beta\cdot r_2^4}\right)$$
$$+ [A(2\beta^2-1) + M(\kappa_2+1) - 1]\frac{R}{\beta}\cdot\frac{y}{r^2} + \frac{2AR^2xy}{r^4}$$

$$H_{22} = (1+\kappa_1)\cdot\theta_1 - 2\frac{x_1 y}{r_1^2} + (A\kappa_1 + B)\cdot(\theta-\theta_2) + \frac{A(2xy-R^2)}{r^2} + 2A\frac{x_2\cdot y}{r_2^2}$$
$$+ \frac{A(\beta^2-1)\cdot R}{\beta^3}\left(-2\beta^2\frac{x_2}{r_2^2} + \frac{(3-\kappa_1)\cdot x_2}{r_2^2} - \frac{4x_2^3}{r_2^4} + \frac{(\beta^2-1)R}{\beta}\left(-\frac{1}{r_2^2} + \frac{2x_2^2}{r_2^4}\right)\right)$$
$$+ [A(2\beta^2-1) + M(\kappa_2+1) - 1]\frac{R}{\beta}\cdot\frac{x}{r^2} + \frac{2AR^2x^2}{r^4}$$

$$\beta = \xi/R, \quad \Gamma = G_2/G_1, \quad A = \frac{1-\Gamma}{1+\Gamma\kappa_1}, \quad B = \frac{\kappa_2 - \Gamma\kappa_1}{\kappa_2 - \Gamma}, \quad C = \frac{\Gamma(\kappa_1+1)}{(\Gamma+\kappa_2)(2\Gamma+\kappa_1-1)}$$

$$M = -\frac{1}{\beta}\{1 + A[(\kappa_1-1)\beta^2 + 1] - C(\kappa_2+1)\}, \quad x_1 = x-\xi, \quad x_2 = x - R^2/\xi, \quad y_1 = y_2 = y$$

$$r^2 = x^2 + y^2, \quad r_1^2 = x_1^2 + y_1^2, \quad r_2^2 = x_2^2 + y_2^2, \quad \theta = \tan^{-1}(y/x), \quad \theta_2 = \tan^{-1}(y/x_2).$$